Uranium in Groundwater: Mechanisms and Rates of U(IV) Mobilization as a Prerequisite for Drinking Water Management

Final Report

By

Kyle J. Chardi, M.Eng.

Supervisors:
University of Vienna: Prof. Dr. Stephan M. Kraemer
Washington University in St. Louis: Prof. Dr. Daniel E. Giammar

University of Vienna

2020

Table of Contents

Abstract

Microbial reduction of soluble hexavalent uranium (U(VI)) to sparing soluble tetravalent uranium (U(IV)) has been utilized as an *in situ* remediation strategy to immobilize U. The presence of organic ligands that can complex both U(IV) and U(VI) is a potential hindrance to the success of such remediation efforts. In the current work, a set of structurally diverse organic ligands were shown to enhance the dissolution of crystalline uraninite for a wide range of ligand concentrations under anoxic conditions at a pH of 7. Comparisons were then made to ligand-induced mobilization of non-crystalline U(IV). For both uraninite and non-crystalline U(IV), aqueous U concentrations remained consistently low in the absence of organic ligands under anaerobic conditions (below 25 nM for UO_2 and 5 nM for non-crystalline U(IV)), highlighting the stability of these forms in the absence of a ligand or oxidant. Yet the addition of a number of different organic ligands (DPA, DFOB, HBED, and citrate) were all able to mobilize U to varying extents. Non-crystalline U(IV) was shown to mobilize substantially more U(IV) at the same ligand concentrations. The ligands mobilized 0.3 % of the UO_2 and 4.6 % of the non-crystalline U(IV). While the bulk remained intact, the mobilized fraction still exceeds drinking water limits, in some cases by several orders of magnitude. Further work was done with reduced field sediments with a variety of organic ligands, highlighting the lability of U(IV) after bioremediation practices and the subsequent susceptibility of the U to remobilization, as seen in batch as well as in a flow-through column experiment with DTPA. The findings of this work show the propensity for numerous organic ligands present in the environment to mobilize both recalcitrant and labile reduced U(IV) species to hazardous levels which should be factored into site characterization and remediation efforts by drinking water management facilities.

Introduction

Uranium (U) is the most commonly found radionuclide in groundwater, soils, and sediments at U.S. Department of Energy (DOE) contaminated sites[1] and poses environmental and human threats globally. Hazardous levels of U in the environment are derived from both anthropogenic sources (mining, ore processing, nuclear fuel, and weapons production) as well as geogenic sources (natural weathering of U-bearing rocks such as granite, limestone, and argillaceous shale).[2, 3] These sources can result in U concentrations in drinking water wells exceeding drinking water quality guidelines, such as the World Health Organization (WHO) guideline value for uranium of 30 µg/L.[4]

The mobility of U is strongly affected by its oxidation state, with hexavalent uranium (U(VI)) species being significantly more soluble than tetravalent uranium (U(IV)) under most environmental settings.[5] Microbial reduction of soluble U(VI) to sparingly soluble U(IV) is utilized as an *in situ* bioremediation strategy for immobilization of U in contaminated aquifers.[6-8] This approach has yielded promising results when it has been employed at numerous field sites such as the Rifle, Colorado site.[9-12]

The chemical composition of groundwater and the localized subsurface environment can jeopardize the stability of immobilized U(IV) species. One of these U(IV) species, uraninite (UO_2), has been found in remediated sediments and is also a major constituent of ores and spent nuclear fuel that will be placed in geologic repositories.[13-16] Dissolved oxygen and nitrate facilitate UO_2 dissolution through oxidative processes on the mineral surface.[17-19] Dissolved inorganic carbon also promotes the dissolution of UO_2 at circumneutral pH under both reducing and oxidizing conditions.[18] Additionally, interaction with other poorly soluble minerals, such as MnO_2, have been shown to substantially increase dissolution rates of UO_2.[20]

Recent research has shown that the product of U(VI) bioreduction includes not only the stable crystalline mineral phases such as UO_2 but also non-crystalline U(IV) species.[21, 22] Non-crystalline U(IV) is operationally defined as U(IV) species for which the U EXAFS (extended X-ray absorption fine structure) Fourier transform spectrum lacks U-U pair correlations characteristic of U(IV) minerals and for which there is no evidence of a crystalline lattice.[21] In many cases, U(IV) is bound to phosphate groups.[23] Furthermore, non-crystalline U(IV) has been found to be substantially more labile than UO_2 due to its

propensity to be readily complexed by bicarbonate[23] as well as be more readily oxidized by O_2 and persulfate[24], with reoxidation by O_2 being accelerated in the presence of FeS.[25] Moreover, aging studies involving a 12 month incubation of bioreduced sediments containing non-crystalline U(IV) were not shown to affect the speciation of U(IV).[26]

Non-crystalline U(IV) has been identified in numerous field locations. For example, it has been found in a naturally U-rich peat soil in an alpine meadow in Switzerland[27] as well as in a wetland impacted by uranium mining activities in France.[22] Additionally, it was identified in naturally reduced sediments in the Colorado Plateau, USA[14] as well as in remediated sediments in the same region.[28-30] Hence, mounting evidence illustrates that the distribution of non-crystalline U(IV) species may be significantly more extensive than previously regarded.

These recent findings in regard to the susceptibility of U(IV) solubilization raise further questions pertaining to the mobility of reduced uranium species in the environment. Yet these works have primarily focused on the susceptibility to oxidative effects of reduced U(IV) species with less work probing the effects of mobilization of U(IV) in the absence of reoxidation. One such notable area of interest is mobilization by organic ligands. Organic ligands have been shown to increase the solubility and dissolution kinetics of tetravalent actinides; such as assessing the effect of citrate, DTPA, DFOB, and other ligands on the mobilization of PuO_2.[31] DFOB has also been shown to increase UO_2 dissolution rates under reducing conditions.[32] Additionally, citrate and EDTA were shown to increase the solubility and dissolution rates of U(IV) under reducing conditions in sediments.[33]

These structurally diverse metal-binding organic ligands play unique roles in the environment. The current study focused on a particular set of ligands. Desferrioxamine (DFOB), a trishydroxamate, is a biogenic Fe-binding microbial siderophore.[34] 2,6-pyridinedicarboxylic acid (DPA), a compound with pyridine and carboxyl functional groups, is a low-molecular-weight organic acid that is a natural product of bacterial sporulation (*Bacillus* and *Clostridium*) providing protection from unfavorable environmental conditions (e.g. heat, UV, heavy metal stress, nutrient limitation)[35], constituting up to 15% of the dry weight of bacterial spores.[36] Citrate, a triscarboxylate, is a low-molecular-weight carboxylate that is ubiquitous in nature.[37] Synthetic ligands are released in industrial or agricultural contexts to the environment. For example, N, N'-di

(2-hydroxybenzyl)ethylene-diamine-N, N'-diacetic acid (HBED), which containins phenol, amine, and carboxyl groups, is a synthetic chelator able to enhance Fe bioavailability[38]. It is commonly used in agriculture in Fe fertilizers to mitigate diminished Fe availability due to poor solubility of Fe(hydr)oxide minerals at circumneutral pH in calcareous soils.

The aims of this study were (1) to systematically evaluate the relative effectiveness of different organic ligands in mobilizing U(IV) from UO_2, (2) to investigate ligand-induced mobilization of non-crystalline U(IV), and (3) assess the effects of organic ligands on U remobilization from a bioreduced field sediment in batch and flow-through configurations. These aims allowed comparison of effects of different ligands on ligand-facilitated dissolution of UO_2 and assessment of the relative stability of non-crystalline U(IV) and UO_2. There have been a limited number of studies which draw direct comparisons between the two materials.[24, 39] While Cerrato et al. compared the release of U from these materials through extractions into water-soluble, ion exchangeable, amenable to complexation by a ligand, and oxidizable fractions, there has yet to be a study to assess the effects of organic ligands. Furthermore, comparisons could then be drawn between U mobilization in pure systems compared to a complex field sediment with other metals present to compete for ligand complexation.

There remain significant knowledge gaps pertaining to the mobility of U(IV) in the environment, specifically in regard to mobilization by organic ligands. A deeper understanding of the mobility of tetravalent U in the environment, and the parameters that control it can contribute to the scientific basis for the design of remediation strategies and predictions of uranium mobility in contaminated subsurface environments and geologic repositories.

Materials and Methods

Material Synthesis

Chemogenic UO_2 was synthesized following the protocol described in Ulrich et al., for which the details are described in full in the Supporting Information (SI).[39] Briefly, studtite was precipitated by mixing H_2O_2 with UO_2Cl_2 and subsequently reduced to UO_2 by $H_{2(g)}$ at 400 ºC for 4 h in a stainless-steel reactor. Non-crystalline U(IV) was synthesized by first producing biomass-associated U(IV) as described in Bernier-Latmani et al.[21] *Shewanella oneidensis* MR-1 cultures were grown in sterile Luria-Bertani broth (LB medium) until reaching midexponential phase. Cells were then harvested by centrifuging at 8,000 RCF for 10 min and washed in a sterile anoxic phosphate-containing medium (WLP) before being resuspended in WLP amended with PIPES, bicarbonate, and lactic acid, and 1 mM uranyl acetate (Table S1).[40] After 15 days of reduction, batch reactors of non-crystalline U(IV) were subsampled for the dissolved U concentration to confirm the extent of bioreduction.

UO_2 Characterization

X-ray powder diffraction (XRD, Bruker d8 Advance powder diffractometer with a Cu Kα X-ray source and a LYNXEYE XE energy-dispersive strip detector) was used to characterize the freshly prepared UO_2. To prevent oxidation of the material during the measurement, the sample was loaded in a silicon zero diffraction plate and enclosed in an anoxic dome inside an oxygen-free glove box. The dome, which is amorphous and transparent to X-rays, remained over the sample as it was analyzed. The resultant pattern from 8º to 17º 2θ is attributed to the anoxic dome. The XRD pattern for UO_2 aligned well with the International Center for Diffraction Data ICDD reference pattern (ICDD 00-041-1422) (Figure S1).

The specific surface area (SSA) was estimated based on the UO_2 density and the size and shape of the UO_2 crystals determined using scanning electron microscopy (SEM, FEI Nova Nano 230) (Figure S2). The particles were measured using the imaging software ImageJ with fifty particles being measured and averaged to yield the 112 nm average size. Particles were assumed to have a cubic shape and a density of 10.99 g cm^{-3},

consistent with published data.[39, 41] The resulting calculation of SSA of 4.9 m^2 g^{-1} is consistent with supporting literature studies from BET and SEM analysis.[39, 42]

Ligand Mobilization Experiments with UO_2 and Non-crystalline U(IV)

The effect of organic ligands on U(IV) mobilization was studied for chemogenic UO_2 and biogenic non-crystalline U(IV) suspensions (300 µM U) at ligand concentrations of 5 µM, 50 µM, 500 µM, and 2 mM for UO_2 and at 50 µM for non-crystalline U(IV). These concentrations aimed to bracket the available surface site concentration from the surface site density of 1.3 µM sites (based off of a SSA of 4.9 m^2 g^{-1} and site density of 2.3 sites nm^{-2}) and a 1:1 U:ligand concentration of 300 µM. Control treatments for UO_2 experiments were conducted in duplicate over two separate experiments with the final result being an average of four replicates with error bars indicated by the standard deviation across all four.

Mobilization experiments were conducted in an anaerobic chamber (Coy Laboratory Products Inc.) containing a gas mixture of 95% $N_{2(g)}$ and 5% $H_{2(g)}$. Gas phase O_2 concentrations were monitored and controlled to be less than 1 ppmv. Batch reactors (polypropylene, 100 mL) were wrapped in aluminum foil to prevent any photochemical reactions. All UO_2 experiments were done in duplicate while only single experiments were performed for non-crystalline U(IV). The pH of all solutions and suspensions was monitored for each sampling timepoint with a pH electrode and meter (Accument XL 15, Fisher).

The pH was buffered by 10 mM 3-(N-morpholino) propanesulfonic acid (MOPS, pK_a = 7.28). MOPS was used previously in UO_2 dissolution studies with no observed effect on uranium mobilization.[24, 32, 42, 43] Adjustments to pH were done by adding NaOH or HCl prior to addition of UO_2 or non-crystalline U(IV). NaCl was added as an electrolyte to a final solution ionic strength of 0.01 M. Ligand stock solutions were prepared at a pH close to the experimental pH (ΔpH ± 0.15) before addition to buffer and electrolyte solution. Suspensions were thoroughly mixed on an orbital shaker (New Brunswick Scientific).

A stock suspension of each U material at a concentration 100 times that anticipated for each batch reactor was freshly prepared in an anaerobic chamber for each set of experiments. Prior to the start of each experiment, the material was washed in HCO_3 (1

M for 8 hours for UO_2, 50 mM for 1 hour for non-crystalline U(IV)) to extract any oxidized U(VI) from the material. Due to the increased lability of non-crystalline U(IV), a lower HCO_3 concentration was used at a shorter interval in accordance with other studies to remove U(VI) without solubilizing the non-crystalline U(IV) itself. [24, 44]

The suspension was then centrifuged at 30,000 RCF for 30 minutes in Nalgene Oak Ridge centrifuge tubes (PP) with sealing caps and decanted. This procedure was repeated with anoxic DI water four times to remove the HCO_3. A subsample (in duplicate) was taken from the suspension and digested in 10% HNO_3 at 100 °C for 4 hours and analyzed by inductively coupled plasma mass spectrometry (ICP-MS, NexION 2000) to determine the exact stock suspension concentration. Once each batch reactor was prepared (ligand added and ionic strength and pH fixed), the U suspensions were spiked into the reactor to provide a final U concentration of 300 μM.

Reactors were sampled over time and samples were filtered with 0.025 μm MCE (mixed cellulose ester) membrane filters (25 mm diameter PP filter holder with silicone gasket) at a constant flow rate of 15 mL h^{-1} using a syringe pump (KD Scientific Model 200). Samples were then acidified with trace metal grade HNO_3 for analysis of dissolved U concentrations by ICP-MS.

As a quality control, an unfiltered sample was taken from each batch reactor at the end of each experiment and digested as detailed above to obtain the average total U concentration in each reactor. Additionally, at the end of each experiment, batch reactors were emptied of suspension and oven digested in 10% HNO_3 as described above to quantify the extent of U-material that had stuck to the reactor wall.

All chemicals were purchased from commercial sources and used as received. Deionized water (DI water, resistivity > 18.2 MΩ·cm, Milli-Q, Millipore) was used for all solutions and suspensions. All anoxic DI water was purged with $N_{2(g)}$ for a minimum of 6 h before being brought into an anaerobic chamber where it was subsequently purged with a 1 M $FeCl_2$ solution through a desiccant for another 6 hours to scavenge any residual oxygen prior to colorimetric inspection of deoxygenation with ultra-low range dissolved oxygen ampoules (ULR CHEMets) to ensure all oxygen had been purged.

Mobilization Rate Calculation

Ligand-promoted dissolution can be described by a rate law in which the ligand promoted dissolution rate is a linear function of the adsorbed ligand concentration at conditions far from equilibrium solubility of the mineral[45]:

$$R_L = k_L \cdot [L]_{ads} \quad (1)$$

In equation 1 R_L is the ligand promoted dissolution rate (nmol h^{-1} m^{-2}), k_L is the first order rate constant (h^{-1}), and $[L]_{ads}$ is the adsorbed ligand concentration (nmol m^{-2}). In the current work dissolution rates were determined without considering possible adsorbed complexes, thereby slightly underestimating dissolution rates.[46] Rates (heretofore referred to as mobilization rates for comparisons made between crystalline UO_2 and non-crystalline U(IV) which does not have a discrete solid surface to dissolve) were calculated for each ligand and concentration with UO_2 by a linear regression approach by observing changes in soluble concentrations of U over time in batch experiments. Rates were calculated for all ligands from 0 – 11 d of the experiment.

Equilibrium Modeling

Equilibrium modelling of UO_2 solubility ($UO_{2(am)}$) under experimental conditions was performed in Visual MINTEQ. Most ligands in the study do not have reported stability constants with U(IV), with the exception of citrate. In the case of citrate, modeling was prepared based off of known constants (Figure S4). All constants used in the model are summarized in Table S2.

Reduction and Subsequent Ligand Remobilization of Uranium in Flow-through Columns & Characterization

Anoxic field sediment and water samples from Retz, Lower Austria were collected where they were anoxically stored until use. Subsequent analysis of samples was done to match the field sediment to an accurate artificial groundwater (AGW) composition for all proceeding experiments. This solution consisted of 7.0 mM $NaHCO_3$, 2.0 mM $CaCl_2$, and 3.2 mM Na_2SO_4 (Table 1). Column experiments were then conducted to mimic U bioremediation efforts at field sites in flow-through conditions. Glucose ($C_6H_{12}O_6$), which was preliminarily shown to successfully reduce U in batch experiments, was used in flow-

through column experiments to stimulate the native microbial community. All solutions were prepared anoxically and pumped into gas resistant bags (Tedlar). Solution pH was buffered to 7.1 ± 0.05 by sparging the solution with $CO_{2(g)}$ to match the native field site pH.

15 cm long glass columns with inner diameter of 25 mm (Diba, OmniFit) were dry-packed with 90 g of anoxic reduced sediment in an anaerobic chamber (Braun Unilab Pro) to approximately 11 cm in length. Columns were wrapped in aluminum foil to avoid phototrophic growth as well as photochemical reactions. Anoxic solutions were pumped upward through the column from the solutions stored in gas-tight bags by a peristaltic pump (Gilson, Minipuls 3) set at 1.5 RPM and the effluent was collected with a fraction collector (Omnicoll) after passing through an inline 0.45 µm cellulose-acetate filter and subsequently diluted and acidified to 1% HNO_3 prior to analysis on ICP-MS.

Columns underwent a number of different phases (i.e. influent solution compositions) throughout the duration of the experiment. Phase 1 was intended to saturate all void volumes of the sediment with the anoxic solution prior to adding the U and glucose. After 10 pore volumes (approximately 3 days), the solution was switched to Phase 2 in which 25.0 µM U and 4.0 mM glucose were added to the AGW solution. Phase 3 continued the addition of 4.0 mM glucose to AGW without U to remove aqueous U(VI) as well as further reduce the remaining U in the column. After the completion of Phase 3, one column was removed and stored in an anaerobic chamber where it was subsequently opened and the sediment was sequestered into five distinct sections for every 2 cm of the column length (sample 1 corresponding with the top of the column and increasing downward against the flow direction). The sediment was then dried and stored in the anaerobic chamber.

Another column continued to run after a Phase 4 solution in which 1 mM of the organic ligand DTPA was added to the AGW. This solution was pumped through the column for approximately 80 pore volumes and effluent concentrations were continued to be monitored to see the effect of the ligand on U and other reduced metal species in the column. After this time, the column was transferred to the anaerobic chamber and stored, dried, and sequestered in the same way as the aforementioned column stopped after Phase 3.

A U-specific sequential chemical extraction was carried out which was modified from Noël et al. 2019 and Jew et al. 2020.[47, 48] The protocol was used for two columns: one after U reduction (Phase 3) and one after remobilization by a ligand (Phase 4). The six-step extraction protocol targeted different pools of U of increasing recalcitrance by each extraction step (Table 2). The extraction was carried out for all five sections along the column length of each column with 1 g sediment, each in triplicate. Sediment from each layer was thoroughly homogenized without destructively breaking down naturally occurring aggregates.

Batch Ligand Remobilization of U(IV) from Reduced Sediments

A subset of the reduced column sediment (comprised of a homogeneous mixture equal parts mixture of sediment from column sections 2 – 4) after U reduction (Phase 3) was used for ligand remobilization batch experiments. Batch experiments were carried out at 5 g L^{-1} SSR in the presence of the same AGW as in the flow-through system (Phase 1). Due to the significantly lower SSR in batch compared to column experiments, thereby diminishing the natural buffering capacity of the sediment, 10 mM MOPS was added to the AGW to stabilize the pH. Numerous organic ligands at varied concentrations were then tested for their ability to mobilize the reduced U accumulated in sediments. Ligands tested were DTPA, HBED, and DPA at ligand concentrations of 0.1, 0.5, and 1.0 mM.

Reduced sediment was pre-saturated in AGW for 12 hours prior to the start of the experiment to equilibrate the sediment with the groundwater composition and ionic environment before ligand addition.[49] This slurry was then added to ligand-containing reactors of AGW and MOPS at time t = 0.

For each timepoint a subsample was taken and centrifuged at 5,000 RPM for 10 minutes prior to filtration with a 0.45 µm cellulose-acetate filter. Filtrate was then acidified to 1% HNO_3 for analysis on ICP-MS.

Results and Discussion

Ligand-induced Mobilization of UO_2

Batch mobilization experiments were conducted to elucidate the chemical mechanisms of UO_2 mobilization by organic ligands (Figure 1A-D). Over the 45 day experiment, the dissolved U concentrations in the control treatment remained relatively constant, ranging between 10 – 25 nM. These values are within an order of magnitude of the predicted equilibrium of 3 nM U from thermodynamic modeling of the $UO_{2(am)}$ solubility under the experimental conditions. These results coupled with the 1 M $NaHCO_3$ rinsing prior to starting the experiment reaffirms that the subsequently presented ligand mobilization results were not enhanced by the presence of trace U(VI) in solution or sorbed to the mineral surface. Small deviations from predicted U concentrations are attributed to minor differences in K_{sp} between the synthesized mineral and that reported in literature (Table S2).

The four tested ligands mobilized U to varying extents and at differing rates (Figure 1A-D). Ligand-induced mobilization of UO_2 proceeded as a slow release mechanism, remaining relatively linear over the experimental duration until the final sample point, in which U concentrations for all ligands except citrate appeared to begin to level off. DPA was the one exception to the linear slow release, in which it exhibited a two-phase mobilization characterized by an initial swift mobilization followed by a slower linear release. Calculated mobilization rates were normalized to UO_2 surface area as well as mass (Table S3). Mobilization rates were further plotted as a function of ligand concentration in solution (Figure 2).

<u>DFOB</u>

The rate and extent of DFOB-induced mobilization of UO_2 increased with increasing ligand concentration, albeit disproportionately to increase in ligand concentration (Figure 1A). The strongest effect was seen between that of the 5 µM treatment which mobilized negligibly more compared to the control treatment and 50 µM which exhibited an increase in both maximum mobilized U concentration and mobilization rate by approximately a factor of 5. Subsequent increases in ligand concentration resulted in increases in U

mobility and mobilization kinetics to decreasing extents up to 2 mM DFOB concentrations. In previous research DFOB adsorption onto UO_2 was found to follow a Langmuir type relationship with surface saturation being reached above approximately 100 µM DFOB.[32] Application of the isotherm parameters from Frazier to the experimental parameters of the current work show surface saturation being reached at much higher DFOB concentrations, approximately an order of magnitude higher at approximately 1,000 µM DFOB (accounting for the differences in SSR and SSA). This supports the findings of decreasing extents of U(IV) mobilization seen proportional to increases in ligand concentration at the higher concentrations tested.

Electrostatic attraction occurs between the UO_2 surface (point-of-zero-charge (PZC) = 5.4) and DFOB at pH 7 (pK_{a1} of DFOB = 8.3; dominant species: H_4DFOB^+), indicating a greater affinity for adsorption for DFOB than the other ligands in the study (all of which are negatively charge at pH 7, similar to the UO_2 mineral surface). Yet Frazier et al. found DFOB adsorption to UO_2 to be constant between pH 3 and 8 despite the change in the surface charge of UO_2, suggesting that electrostatic interactions only impart a small contribution on DFOB adsorption to the UO_2 surface.

Further comparisons and insights can be made between the present study and the work of Frazier et al. in which similar experiments were conducted with UO_2 and DFOB. Specifically, both studies observed increased mobilization of U(IV) in the presence of DFOB, as well as increasing rates of release with increasing DFOB solution concentrations. In both studies, DFOB did not completely dissolve the bulk UO_2 (while Frazier worked with lower overall ligand concentrations, greater SSR of 0.35 g L^{-1}, and with a UO_2 with slightly lower specific surface area of 3.94 m^2 g^{-1}). Yet the extent and rate of mobilization do not match one another. Frazier observed dissolved U concentrations as high as 10 µM with 20 µM DFOB addition and over 60 µM U with 200 µM DFOB.[32] The discrepancy between the significantly higher dissolved U concentrations found in their work and our current results (surface-saturated net dissolution rate of 64 nmol h^{-1} m^{-2} from 100 µM DFOB and 1.0 g L^{-1} UO_2 in CFSTR experiments in Frazier compared to 2.5 nmol h^{-1} m^{-2} from 2 mM DFOB and 0.1 g L^{-1} UO_2 in batch experiments in the current work (Table S3)) are hypothesized to be due to a number of different factors. First, the mineral synthesis process was not the same, yielding a less crystalline product (which could in

turn increase dissolution rates) in Frazier et al., which yielded less defined and sharp peaks in comparison to the ICDD XRD reference pattern. Second, the lack of a bicarbonate washing step prior to the experiment could have allowed some U(VI) to remain on the mineral surface. Ligand-free control experiments by Frazier exhibited U concentrations at least five times higher than those in the control experiments of the current study. Another contributing factor to the greater extent of mobilization seen in Frazier et al. is that the adsorbed ligand concentration in their work was higher than what was calculated in the experiments of the current study, enabling greater ligand promoted dissolution rates with increased available surface sites at like-concentrations of DFOB.

DPA

DPA (Figure 1B) was the most effective ligand at mobilizing U from UO_2. DPA mobilized over 750 nM U with as low as 5 µM DPA addition. DPA exhibited a unique and striking result of showing very minimal ligand concentration dependency, mobilizing less than 200 nM more U at a ligand concentration of 2 mM compared to at 5 µM. Given the sparse research on U(IV)-DPA complexation, comparisons were made to other tetravalent actinides and Fe(III)-DPA complexes. Np and DPA were found to complex in a 1:3 ratio with DPA anions acting as tridentate ligands.[50] DPA is known to provide electron density to actinides by two carboxylate O and one aromatic N.[51] Notably, U(IV)-DPA complexes were found to form nine-fold coordination to U. This has been seen through complexes with 1:2 U:DPA coordination with each DPA ligand acting as a tridentate connector with three additional O atoms from water molecules complexing.[52] Other studies have found 1:3 U:DPA coordination, forming a tricapped trigonal prismatic configuration (coordination number = 9).[53] While the exact coordination is still unknown, the striking mobilization effect seen with DPA even at low ligand concentrations on the recalcitrant UO_2 points towards a swift detachment of the U(IV)-DPA complex from the surface of the crystalline lattice, highlighting the need for further investigation of the U(IV)-DPA complex.

HBED

The strong synthetic iron chelator HBED (Figure 1C) only minimally enhanced UO_2 dissolution with dissolved U concentrations peaking at less than 150 nM U for 2 mM

HBED. It is notable that while HBED showed a clear concentration dependency on U mobilization (if to a much lower extent of U mobilization), a clear inhibitory effect was observed at the lowest ligand concentration of 5 µM. This treatment consistently mobilized less U than the control (Figure S3). One hypothesis could be that there is ample adsorption by HBED to the surface and that any complexes formed by HBED also favor the surface. Yet if too many complexes form without destabilizing the mineral structure, sorbed ligand complexes would not be able to detach from the surface and dissolve into solution. In this case, the large hexadentate sorbed ligand could create a shielding effect not exhibited in control treatments but when higher ligand concentrations are added there is an excess of available dissolved HBED to drive dissolution of U(IV)-HBED complexes into solution.

Citrate

Uranium mobilization from UO_2 by citrate (Figure 1D) demonstrated two distinct patterns. The lower ligand concentrations (5 µM, 50 µM) had a concentration dependency (albeit still below 150 nM maximum mobilized U concentration) with the 5 µM treatment mobilizing only slightly more than the control and 50 µM mobilizing only marginally more. A clear distinction is seen though with the higher ligand concentrations (500 µM, 2 mM) with U mobilization consistently scaling approximately three times higher than that of the 50 µM treatment for both higher concentrations. Furthermore, virtually no difference was seen between the two higher ligand concentration treatments, alluding to a saturation of the UO_2 surface with citrate. While both 1:1 and 1:2 U(IV)-citrate stoichiometries have been observed by spectrophotometric measurements, there has yet to be an EXAFS study to confirm such complexes.[54]

Equilibrium modelling of UO_2 solubility ($UO_{2(am)}$) under experimental conditions for citrate were conducted in Visual MINTEQ (Figure S4). Although the latest revisions to the NEA database were unable to select a single recommended value for the 1:1 U(IV)-citrate complex, the provided constants in the NEA[55] and other literature studies[54] were each tested against experimental results (Table S2). In each case, the modelled results showed negligible U mobilization up to the highest experimental ligand concentration of

2 mM at pH 7 resulting in significantly under-predicting the mobilized U concentrations seen in Figure 1D.

Luo et al. previously tested the ability of citrate to mobilize U from biologically reduced sediments from the Y-12 Oak Ridge, TN field site (nanoparticulate UO_2 or associated with iron-oxide minerals) in batch studies. In their work, Luo et al. found citrate to mobilize U(IV) to similar nM levels as in the current study at concentrations of 700 µM and 1.4 mM citrate yet at much lower total U concentrations (0.8 g kg^{-1} of solids at 2 g L^{-1}; ~7 µM).[33, 56]

The observed differences in mobilization patterns between ligands can be attributed to numerous factors: specificity of ligand for target metal (charge-to-radius ratio, electronegativity, polarizability) and geometry of ligand and binding moieties (nature and number of binding sites, ion size and electron configuration of metal ion, ligand geometry and structural flexibility), for example. U^{4+} is a hard acid ion, with a high ionic potential, high electronegativity, and low polarizability; demonstrating a high affinity for hard ligating groups, containing donor atoms such as oxygen, and commonly forming coordinative bonds with more ionic character. [57, 58]

Electrostatic interactions can play an important role in metal-ligand complexation, with ions which adsorb relatively poorly by electrostatic attraction typically forming weaker outer-sphere complexes.[59] The dominant speciation for each ligand at the experimental pH were probed for correlations to mobilization rates. For the current study, each ligand exhibited a different net proton charge at pH 7 (H_4DFOB^+, DPA^{2-}, H_3HBED^-, $citrate^{3-}$) while the point-of-zero-charge (PZC) for UO_2 is 5.4, resulting in a negative surface charge at pH 7, favoring adsorption of cations [60]. There does not appear to be a clear trend in mobilization pattern for each ligand compared to the net proton charge at pH 7, indicating that the coordination could be driven by more geometric compatibilities. The ligands in this study fall into two coordination categories: DFOB and HBED are both hexadentate ligands while DPA and citrate are both tridentate ligands.

Equilibrium Modeling of UO_2

While the material in Luo et al. greatly differs from the pure mineral chemogenic UO_2 of this study in a plethora of ways associated with heterogeneity of field sediments and

microbially mediated reduction processes, both studies found citrate to mobilize substantially more U experimentally than predicted by equilibrium modeling using current thermodynamic constants for U(IV)-citrate complexation. In both cases, models determined $U(OH)_4$ to be the dominant aqueous U((IV) species at experimental pH (6.5 and 7.0 for Luo et al. and the current study, respectively). This could be attributed to a 1:3 U(IV):citrate complex that drives U(IV) mobilization above UO_2 solubility for which there are currently no constants. There are currently no reported studies which define stability constants for U(IV) with the other ligands in this study. The underpredictions by thermodynamic models for U(IV)-citrate complexation in multiple and varied setups in conjunction with the aforementioned diverse group of organic ligands able to mobilize UO_2 above drinking water standards which currently have no U(IV)-ligand stability constants exemplifies the need for further investigation into the reactivity of reduced U(IV) species with organic ligands to facilitate better preventive measures at field sites as well as improve modeling applications.

Ligand-induced Mobilization of Non-crystalline U(IV)

Investigation of non-crystalline U(IV) solubilization with 50 μM DFOB, DPA, and HBED as well as a control treatment with no ligand addition were carried out as single experiments (Figure 3). Non-crystalline U(IV) experiments were run for a shorter duration than UO_2 at 9 days to avoid possible effects of biomass degradation on the material. Over the 9 day experiment, the control treatment remained low, with dissolved U concentrations ranging between 2 – 5 nM. The sustained low concentrations observed (notably lower than for crystalline UO_2) throughout the experiment support the findings that oxidative effects did not contribute to the observed mobilization effects. For reference, Cerrato et al. determined that nearly 100% of non-crystalline U(IV) ould be oxidized by 8.2 mg L^{-1} dissolved oxygen within four hours.[24]

Both the extent of U mobilization and the rate of U mobilization were larger for non-crystalline U(IV) in comparison to UO_2 for the three ligands tested. Interestingly though, when comparing ligand mobilization for a specific ligand for each material, there was not a general relationship that could be applied. DFOB mobilized twice as much U from non-crystalline U(IV) than from UO_2 at equal ligand concentrations of 50 μM. HBED, which

was notably less potent for mobilizing U from UO_2, was able to mobilize over 3 μM U within four hours of non-crystalline U(IV) addition, which is almost two orders of magnitude higher mobilization compared to UO_2 at equal ligand concentrations over the experimental duration. DPA, on the other hand, exhibited a similar trend as with UO_2 in which it had a fast initial release compared to the other ligands tested and then leveled off, mobilizing over an order of magnitude more U(IV) than from UO_2. These results show that, while non-crystalline U(IV) is extremely labile and susceptible to mobilization, in the absence of complexants and oxidants its solubility is extremely low.

The findings of this work point towards a fast mobilization effect, reaching equilibrium within the first 1 - 2 days. Yet even with these strong mobilization effects, the bulk of the non-crystalline U(IV) was not mobilized. This is hypothesized to be in part due to competition between ligands and biomass for binding U(IV). Experimental findings do suggest though that a larger fraction of the total U is available for complexation in non-crystalline U(IV) compared to UO_2.

The extent of U release for both materials tested yields similar results as the chemical extractions carried out in Cerrato et al. when comparing the relative percentages of U released for the different loadings. In their work, Cerrato et al. found that when carrying out extractions of U(IV) species amenable to complexation by a ligand (0.1 M NaF), that only 1% of UO_2 was extracted and 5% of non-crystalline U(IV) was extracted.[24] While the concentrations of the initial U-containing materials in that work were approximately 5-times higher than those in this work and NaF extractant concentrations were substantially higher than tested ligand concentrations, the overall extent of U mobilized were similar with as much as 0.3% total U mobilized in UO_2 experiments with both DPA and DFOB (at notably higher ligand concentrations than DPA) and as much as 4.6% total U mobilized in non-crystalline U(IV) experiments with DPA (Figure 4).

Remobilization of Uranium from Bioreduced Sediment by Organic Ligands

Uranium Reduction in Bioreduced Sediment Columns

Uranium reduction was seen to take place rapidly after the breakthrough of U from the addition of U and glucose in the P2 solution (Table 1, Figure S5). Iron and Mn were then shown to mobilize after U reduction took place between approximately pore volume 20 –

60. This points towards increasing reducing conditions being reached, as effluent Fe concentrations were shown to match well with Fe(II) measurements using a Ferrozine assay. This would then indicate that during the Fe release that Fe(II) reductive dissolution is taking place from Fe(III)hydr(oxide) minerals and following a redox ladder for the release of each metal (although notable that U comes first in this case, presumably due to its labile state being introduced aqueously compared to Fe and Mn-bearing minerals in the sediment).[61] After this point, dissolved metal concentrations of all metals of interest remained low for the duration of P2 and P3. Uranium reduction was carried out until the calculated accumulation of U within the column averaged across the column length reached 100 mg kg^{-1}.

Batch Remobilization Experiments

Throughout the course of the experiment, the control treatment (in the absence of an organic ligand) fluctuated between 0.01 – 0.4 µM U. The unpredictable nature of the control highlights the environmental complexity of working with field sediments in which diverse and not always easy to interpret biogeochemical processes are taking place concurrently with testing experimental parameters. It further reaffirms that, while U reduction in flow-through columns was successful in reducing influent U(VI) to U(IV), the resultant U(IV) is in a labile pool still susceptible to remobilization from varied sources, even within the AGW (Figure 5, Figure 6). It is notable that in this case, the control treatment elevated soluble U concentrations above even drinking water standards. Regardless of this, each of the tested organic ligands remobilized U beyond the greatest extent seen in control treatments (Figure 7, Figure 8, Figure 9), highlighting the possible injurious result of various organic ligands' presence in the subsurface in the vicinity of reduced U pools.

All three ligands tested remobilized comparable amounts of U but at varied ligand concentrations and exhibiting different mobilization patterns. DTPA and HBED exhibited the same extent of remobilization for 0.1, 0.5, and 1.0 mM ligand concentrations over the first 5 days (Figure 7, Figure 8). In the case of DTPA, U concentrations reached approximately 0.75 µM, while in the case of HBED U concentrations reached approximately 0.55 µM within the same amount of time. As can be seen from the fast

release of U in the control over this timeline, some of this effect is driven by change in electrolyte and solution composition when the sediment was first mixed. This supports the interpretation that the reduced U in more loosely associated with the sediment surface and not structurally incorporated within or forming any crystallinity to hinder the quick release seen.

After the first 5 days an interesting opposing trend is seen between DTPA and HBED. The 0.1 mM DTPA treatment subsequently dropped after this time (mirroring the pattern of the control treatment) and consistently mobilized less than the two other higher DTPA treatments which mobilized nearly the same amount of U throughout the course of the experiment, alluding to surface saturation of the ligand complex being reached. HBED, on the other hand, exhibited nearly the same mobilization pattern for both the 0.5 and 1.0 mM treatments while the 0.1 mM tended to increase more than the other treatments over time. This result is especially fascinating in comparison to the results from UO2 studies in which at lower ligand concentrations (notably lower still than those in this study, at 5 µM) displayed an inhibitory effect on U mobilization (Figure S3). These differing results are interpreted to be due to the competitive effects between other metals, notably Fe in which the 0.1 mM treatment mobilized less Fe over the same time points which it complexed more U.

The remobilization pattern of the DPA treatment differed from the other two ligands in that it was significantly ligand concentration dependent (Figure 9). This could be due to the fact that DPA is a low-molecular weight organic acid while the other two ligands have higher stability constants and known to form stronger complexes with other metals, such as Fe. This concentration dependency resulted in a decrease in the soluble U concentration after the first 5 days for both 0.1 and 0.5 mM treatments (to a greater extent for 0.1 mM). The 1.0 mM treatment remained stable at approximately 0.80 µM U from this point onward, only slightly mobilizing any more U over the course of the following four weeks.

In both UO_2 and non-crystalline U(IV) experiments, DPA mobilized the most U. Furthermore, in the case of UO_2, it was shown to mobilize nearly the same amount regardless of ligand concentration ranging from 5 nM to 2 mM. These findings show the importance of upscaling experimental findings to greater environmental relevance. These

results show that while DPA is still a significantly strong ligand at mobilizing U(IV), when in an environmental system with numerous competing metals for complexation, the extent of its pronounced effects in pure reduced U systems is brought more inline with the other ligands.

Column Remobilization Experiments

To continue to build upon the environmental relevance, a final column experiment was run in which 1.0 mM DTPA was added to the column influent along with the AGW after approximately 150 PV of U reduction (Figure 10). This column went through the same influent solutions (Table 1) and number of pore volumes of each as that of the columns used for producing the sediment for batch remobilization experiments and contains approximately the same amount of total reduced U. After ligand addition (P4), an immediate stark remobilization was seen for U, Fe, and Mn. Remobilized U concentrations peaked at 13 µM, half of the concentration of the input U concentration. This remobilized fraction accounted for 15% of the total accumulated reduced U within the column. In comparison, Fe which peaked at 825 µM yet this only accounted for 0.6% of the total Fe in the column. Interestingly, all three metals mobilized simultaneously at the introduction of DTPA, indicating that there was plentiful DTPA to complex available U, Fe, and Mn.

Sequential Extraction

A sequential extraction was then carried out on the sediment from the U reduction column (Figure S5) as well as the column which had DTPA introduced after P3 (Figure 10) to see the effect of the ligand on the distribution and extent of U within each extractant pool.

Results of the sequential extraction showed that the majority of U was extracted in the second extraction step, an anoxic 1 M bicarbonate extraction (Table 2, Figure 5), targeting the exchangeable phase. This pool targets non-crystalline U(IV) as well as U(IV) and U(VI) which are strongly adsorbed to organic matter or minerals present in the sediment.[44, 47] Section 2 (second from the top) was shown to contain substantially contain the largest fraction of U within the column, notably within extractant 2, with this peak being greatly diminished when compared to the sequential extraction results of the column after

DTPA addition to the influent solution (Figure 6). This diminishment in the peak at section 2 across the columns before and after ligand addition shows that U reduction was significantly localized within the 2 cm layer of this section and that the ligand primarily mobilized this fraction of the reduced U. Yet diminishments were also seen from the pools of extractant steps 3 – 5, alluding to more recalcitrant reduced U species forming which the ligand was subsequently also able to remobilize (Figure 6).

Results of Fe and Mn from the sequential extraction showed that these species were significantly more recalcitrant than those of U, requiring much stronger extractants to release the metal as seen by Fe only starting to be extracted first during the fourth extractant step and primarily being released during the aqua regia digest (extractant 6) (Figure S6). A similar trend was seen with Mn except that the proportion coming out from extractant 4 significantly increased to be approximately 33% of the total with the remainder coming out primarily from extractant 6 (Figure S7).

Environmental Implications

The findings of this work highlight the stark contrast in the susceptibility, extent, and rate of ligand-induced mobilization between chemogenic UO_2 and biogenic non-crystalline U(IV) for a number of different ligands across a wide range of concentrations. The present results demonstrate the ability of organic ligands to mobilize a variety of reduced U species under anoxic conditions. Furthermore, substantially more U was mobilized from non-crystalline U(IV) and at a significantly higher mobilization rate than from UO_2. These conclusions add to the current state of research of the lability of non-crystalline U(IV) in the environment, supporting further investigation into the bioreduction pathways which produce and inhibit its formation, as well as a heightened need to characterize field sites more robustly to account for these variances in the field.

While the extent of ligand-induced U mobilization from non-crystalline U(IV) was substantially more than that from UO_2, it is notable that all ligands tested with UO_2 mobilized U to a level exceeding the WHO maximum contaminant level (MCL) of 30 μg L^{-1} (126 nM). There are additionally a number of countries which have even stricter guidelines (i.e. Canada, 20 μg L^{-1}; Germany, 10 μg L^{-1}).[62, 63]

Further experiments with biogenic reduction of U with field-collected sediments showed that while bioreduction efforts can be effective at mitigating elevated soluble U concentrations during the application of electron donor, that these reduced U pools can still be significantly labile and are susceptible to being remobilized by organic ligands. This was demonstrated in both batch and flow-through column experiments resulting in elevated U concentrations above drinking water standards.

In the context of current regulatory limits, a minimum threshold for each ligand tested can be established from the pure mineral phase presented here and incorporated into predictive models to account for other environmental factors (i.e. oxidants, carbonates, phosphates, iron sulfides, etc.). Furthermore, it has been demonstrated that strong Fe(III)-chelating ligands (such as HBED) do not pose the largest threat for U(IV)-containing solids, and thus, other organic ligands (such as shown in this study with DPA) must be assessed as well.

Based off of these findings, organic ligands present in the environment (even at low concentrations and in field sediments with competing metals to complex with the ligand) pose a threat to even the most recalcitrant reduced U species (UO_2) with increasing severity and concern with more labile reduced U species, such as non-crystalline U(IV) and those with larger surface areas.

Tables and Figures

Table 1. Solution composition breakdown for flow-through column experiments. Depending on the experiment, columns were stopped either after Phase Three to replicate U bioreduction practices or after Phase Four to assess the effect of an organic ligand.

Phase One	Phase Two	Phase Three	Phase Four
AGW	**U-accumulation**	**U-biomineralization**	**Ligand remobilization**
7.0 mM $NaHCO_3$	7.0 mM $NaHCO_3$	7.0 mM $NaHCO_3$	7.0 mM $NaHCO_3$
2.0 mM $CaCl_2$	2.0 mM $CaCl_2$	2.0 mM $CaCl_2$	2.0 mM $CaCl_2$
3.2 mM Na_2SO_4	3.2 mM Na_2SO_4	3.2 mM Na_2SO_4	3.2 mM Na_2SO_4
	4.0 mM $C_6H_{12}O_6$	4.0 mM $C_6H_{12}O_6$	1 mM DTPA
	25 µM U		

Table 2. Sequential extraction steps carried out for U reduction column and column after ligand remobilization. All samples prepared in triplicate with 1 g of homogenized sediment from each section of the respective column.

Extraction step	Extractant	Reaction time
(1) Water soluble	25 mL anoxic ultra-pure water	24 hours
(2) Exchangeable/organics	25 mL 1M anoxic sodium bicarbonate	48 hours
(3) Carbonate	16 mL 1M anoxic sodium acetate	5 hours
(4) Metal oxide/phosphates	20 mL 0.04 M anoxic hydroxylamine hydrochloride in 25% acetic acid	6 hours
(5) Uraninite	25 mL 1M oxic sodium bicarbonate	48 hours
(6) Total digest	12 mL Aqua Regia (3 mL HNO_3, 9 mL HCl)	2 hours

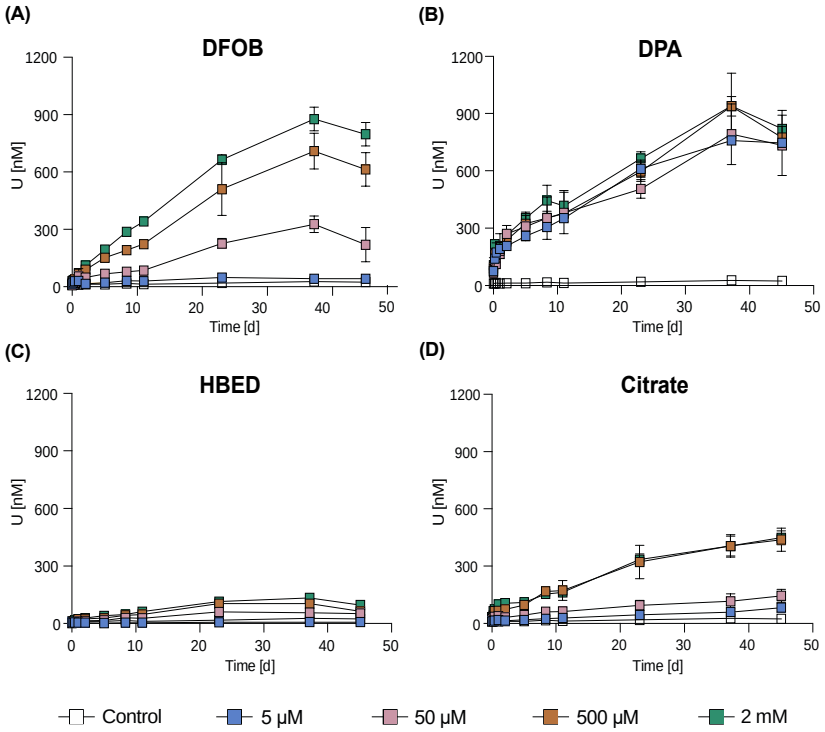

Figure 1. U mobilization from UO_2 (300 µM) induced by (A) DFOB, (B) DPA, (C) HBED, and (D) citrate at concentrations of 5 µM, 50 µM, 500 µM, and 2 mM with a fixed pH of 7. All experiments contained 10 mM MOPS and 6.6 mM NaCl. Control treatment contains same composition of other treatments except without ligand addition. Error bars indicate standard deviation of duplicate reactors. Time t = 0 h corresponds to when an aliquot of the UO_2 stock suspension was added to solution of buffer, electrolyte, and ligand to provide the 300 µM U.

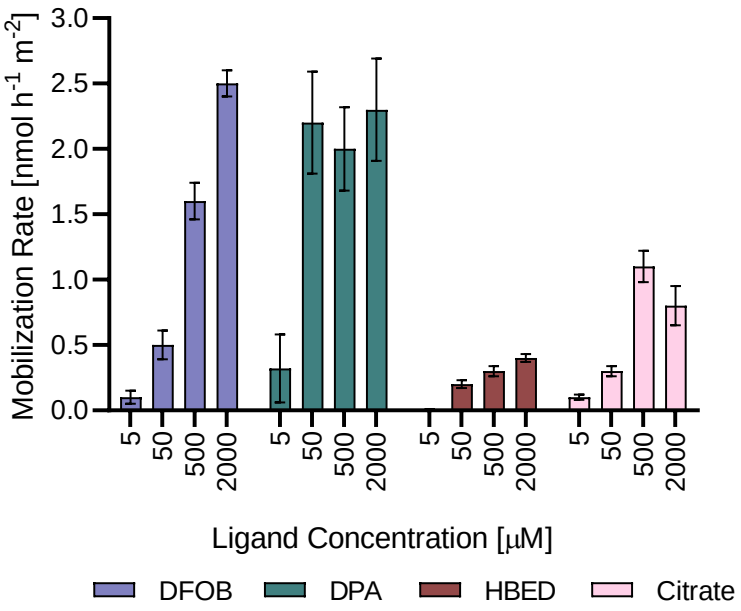

Figure 2. U mobilization rate as a function of ligand concentration in solution for DFOB, DPA, HBED, and citrate. The U mobilization rate in control treatments was 0.03 nmol h^{-1} m^{-2}. Error bars represent standard error of linear regression analysis from batch mobilization data.

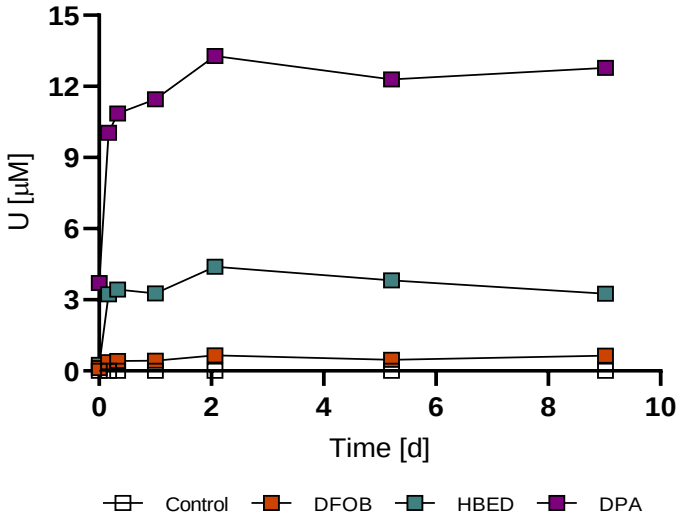

Figure 3. U mobilization from non-crystalline U(IV) (300 μM) induced by 50 μM DFOB, DPA, and HBED, with a fixed pH of 7. Control treatment contains same composition of other treatments except without ligand addition. Error bars indicate standard measurement error from analysis. Time t = 0 h corresponds to when an aliquot of non-crystalline U(IV) stock suspension was added to solution of buffer, electrolyte, and ligand to provide the 300 μM U.

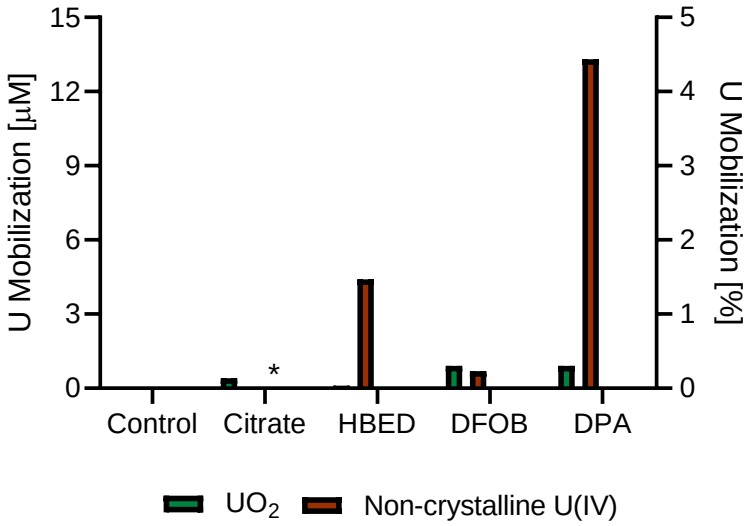

Figure 4. Comparison of total mobilized U from UO_2 and non-crystalline U(IV) batch experiments. UO_2 data reflect peak U concentrations after 45 days at ligand concentrations up to 2 mM while non-crystalline U(IV) data reflect peak U concentration after 9 days at a ligand concentration of 50 µM. Citrate mobilization experiments were not carried out with non-crystalline U(IV), denoted by (*) on the graph.

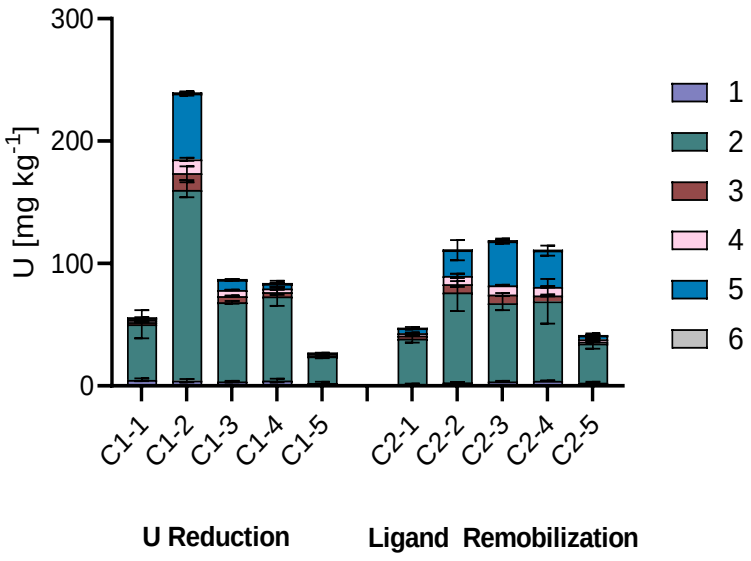

Figure 5. Uranium sequential extraction for U reduction column and column after ligand remobilization. Error bars indicate standard deviation of triplicate reactors. Extractant solutions, SSR, and durations of each step are summarized in Table 2.

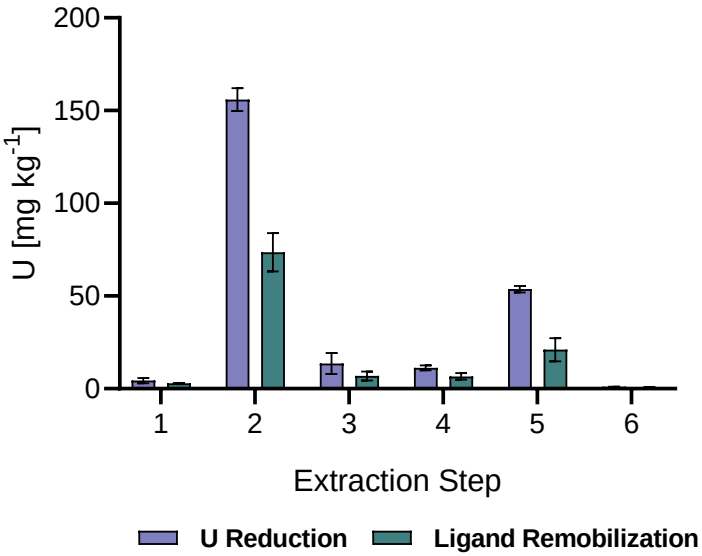

Figure 6. Comparison of extent of U extracted per sequential extraction step for the section of greatest U accumulation (section 2, second from the top) for U reduction column and column after ligand remobilization. Error bars indicate standard deviation of triplicate reactors. Extractant solutions, SSR, and durations of each step are summarized in Table 2.

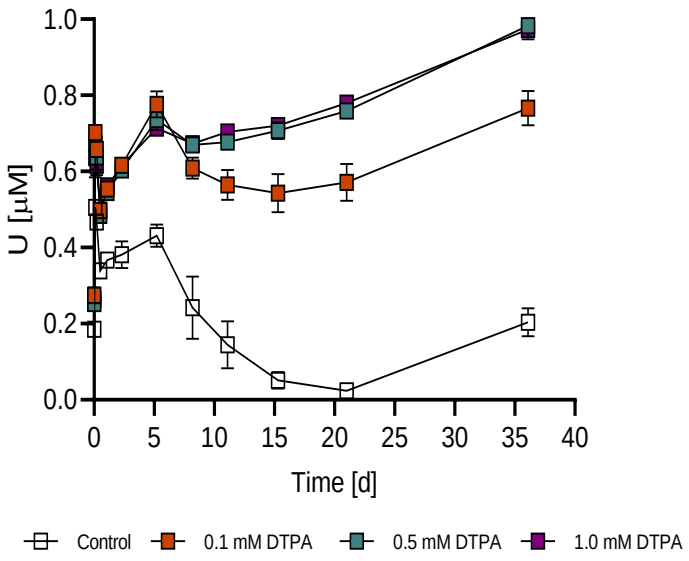

Figure 7. U remobilization from reduced field sediment by DTPA at ligand concentrations of 0.1, 0.5, and 1.0 mM. All experiments carried out with AGW and 10 mM MOPS with pH set to 7.5. Control treatment contains same composition of other treatments except without ligand addition. Error bars indicate standard deviation of triplicate reactors. Time t = 0 h corresponds to when sediment slurry was added to solution of AGW, buffer, and ligand.

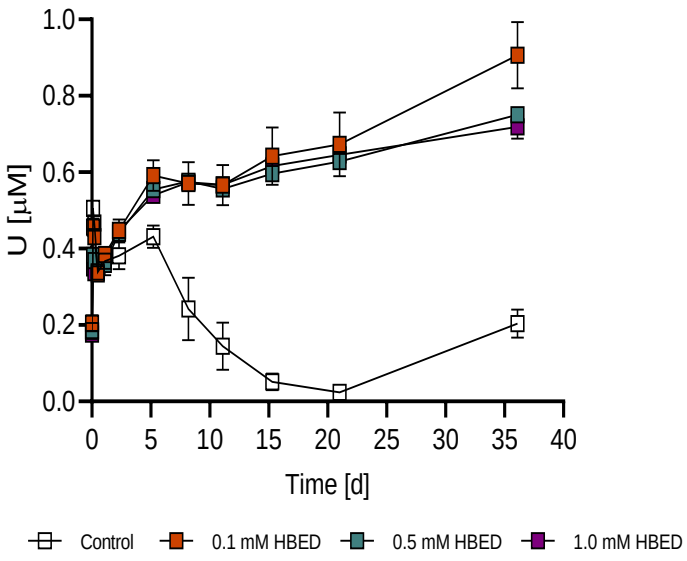

Figure 8. U remobilization from reduced field sediment by HBED at ligand concentrations of 0.1, 0.5, and 1.0 mM. All experiments carried out with AGW and 10 mM MOPS with pH set to 7.5. Control treatment contains same composition of other treatments except without ligand addition. Error bars indicate standard deviation of triplicate reactors. Time t = 0 h corresponds to when sediment slurry was added to solution of AGW, buffer, and ligand.

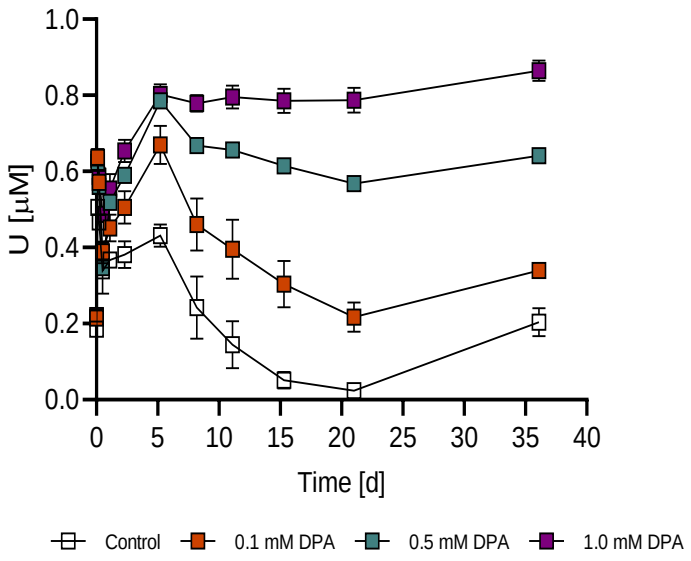

Figure 9. U remobilization from reduced field sediment by DPA at ligand concentrations of 0.1, 0.5, and 1.0 mM. All experiments carried out with AGW and 10 mM MOPS with pH set to 7.5. Control treatment contains same composition of other treatments except without ligand addition. Error bars indicate standard deviation of triplicate reactors. Time t = 0 h corresponds to when sediment slurry was added to solution of AGW, buffer, and ligand.

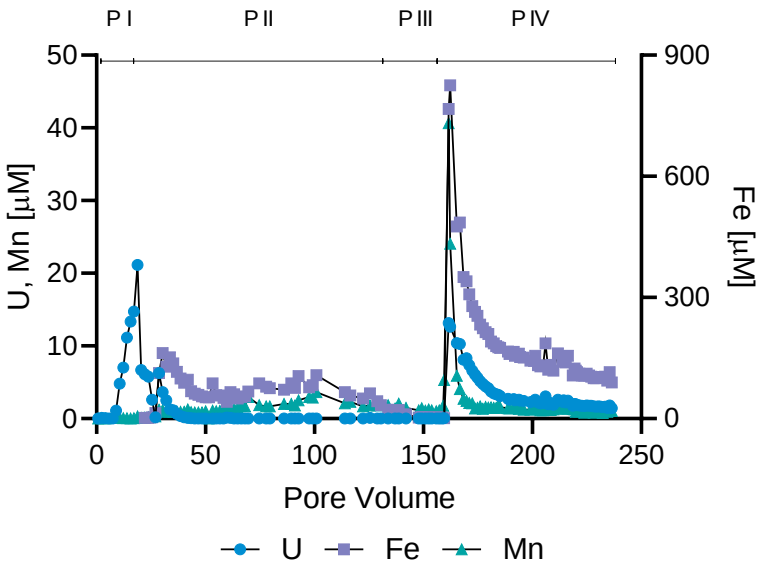

Figure 10. Uranium breakthrough, reduction, and remobilization by 1 mM DTPA. P1 consisted of AGW solution. P2 consisted of AGW plus 4 mM glucose and 25 µM U. P3 consisted of AGW plus 4 mM glucose. P4 consisted of AGW plus 1 mM DTPA. All influent solutions were sparged with $CO_{2(g)}$ to pH 7.1 and pumped into anoxic gas-tight bags. Full influent solution compositions are summarized in Table 1.

Supporting Information

UO_2 Synthesis

UO_2 was synthesized following the protocol described in Ulrich et al., 2008 and summarized below. Uranyl nitrate was heated at 275 °C under oxic conditions for 72 hours in a muffle furnace to remove nitrates and produce $UO_{3(s)}$ (schoepite).

The freshly synthesized $UO_{3(s)}$ was dissolved in 0.5 M HCl to yield a UO_2Cl_2 aqueous solution. This solution was mixed with 30 mL of H_2O_2 in a 3 L HDPE reactor filled to volume with ultra-pure water (UPW) and continuously stirred for 72 hours. A pale-yellow precipitate, uranium peroxide, was then allowed to settle at the bottom of the reactor and the supernatant was discarded. The resultant slurry was dialyzed against UPW for an additional 72 hours. Every 24 hours electrical conductivity (EC) was measured (as an indicator for high ionic concentrations) in the UPW and replaced with fresh UPW. After 72 hours the EC was found to be nearly zero and dialysis was subsequently stopped.

The uranium peroxide precipitate was transferred to a reactor tubes and frozen to -80 °C prior to being freeze dried for 96 hours to evaporate residual water without causing any structural changes to the uranium peroxide.

Dried uranium peroxide was then reduced to UO_2 in a stainless-steel reactor in the presence of $H_{2(g)}$ at 400 °C for 4 hours by use of a cartridge heater and temperature controller. To ensure a continuous supply of $H_{2(g)}$, the reactor was connected on the influent-end to a pressurized hydrogen cylinder and a tubing from the effluent end was inserted in a beaker of UPW to gauge the continuous flow based off of the presence of bubbles. After 4 hours of reaction, the heater was turned off and allowed to cool while $H_{2(g)}$ continued to flow to maintain anoxic conditions within the reactor. Once reaching room temperature, the reactor was transferred to an anaerobic chamber (Coy Laboratory Products Inc.) containing a gas mixture of 95% $N_{2(g)}$ and 5% $H_{2(g)}$. The UO_2 was stored in an amber glass bottle until use.

Table S1. Basal medium composition of Widdel Low Phosphate (WLP) used for synthesis of non-crystalline U(IV).

Compound	WLP (mM)
$CaCl_2 \cdot 2H_20$	0.68
KCl	6.71
KH_2PO_4	0.22
$MgCl_2 \cdot 6H_20$	2.46
NaCl	85.56
NH_4Cl	4.67
$NaHCO_3$	30
PIPES	20
pH	7.3

Table S2. Thermodynamic stability constants (T = 25° C, I = 0) for aqueous and solid phase reactions as used in Visual MINTEQ.

Reaction	Log K	Source
U Hydrolysis		
$U^{4+} + H_2O \rightleftharpoons UOH^{3+} + H^+$	-0.4	1
$U^{4+} + 2H_2O \rightleftharpoons U(OH)_2^{2+} + 2H^+$	-1.1	1
$U^{4+} + 3H_2O \rightleftharpoons U(OH)_3^{+} + 3H^+$	-4.7	1
$U^{4+} + 4H_2O \rightleftharpoons U(OH)_{4(aq)} + 4H^+$	-10	1
$U^{4+} + 2H_2O \rightleftharpoons UO_{2(am, hyd)} + 4H^+$	-1.5	1
U Inorganic Anion Complexation		
$U^{4+} + Cl^- \rightleftharpoons UCl^{3+}$	1.72	1
Citrate Hydrolysis		
$Citrate^{3-} + H^+ \rightleftharpoons HCitrate^{2-}$	6.4	2
$Citrate^{3-} + 2H^+ \rightleftharpoons H_2Citrate^-$	11.2	2
$Citrate^{3-} + 3H^+ \rightleftharpoons H_3Citrate$	14.3	2
U-Citrate Complexation		
$Citrate^{3-} + U^{4+} \rightleftharpoons UCitrate^+$	12.8	3
$2Citrate^{3-} + U^{4+} \rightleftharpoons U(Citrate)_2^{2+}$	19.5	2

(1) Guillaumont et al. 2003[64]

(2) Hummel et al. 2007[55]

(3) Bonin et al. 2008[54]

Table S3. Mobilization rates for DFOB, DPA, HBED, and citrate of UO_2 at treatment concentrations of 5 µM, 50 µM, 500 µM, and 2 mM with a fixed pH of 7 for 300 µM U with SSA of 4.9 $m^2\ g^{-1}$. All rates calculated over the first 11 days of the experiment.

Treatment	nM h^{-1}	nmol $h^{-1}\ g^{-1}$	nmol $h^{-1}\ m^{-2}$	R^2
Control	0.0	0.1	0.0	0.45
DFOB - 5 µM	0.0	0.3	0.1	0.18
DFOB - 50 µM	0.3	2.6	0.5	0.80
DFOB - 500 µM	0.8	7.7	1.6	0.95
DFOB - 2 mM	1.2	12.1	2.5	0.99
DPA - 5 µM	0.8	8.4	1.7	0.88
DPA - 50 µM	1.1	10.9	2.2	0.84
DPA - 500 µM	1.0	10.0	2.0	0.87
DPA - 2 mM	1.1	11.5	2.3	0.86
HBED - 5 µM	0.0	0.0	0.0	0.33
HBED - 50 µM	0.1	1.0	0.2	0.91
HBED - 500 µM	0.1	1.5	0.3	0.90
HBED - 2 mM	0.2	1.8	0.4	0.95
Citrate - 5 µM	0.1	0.6	0.1	0.91
Citrate - 50 µM	0.1	1.3	0.3	0.90
Citrate - 500 µM	0.5	5.4	1.1	0.93
Citrate - 2 mM	0.4	3.9	0.8	0.83

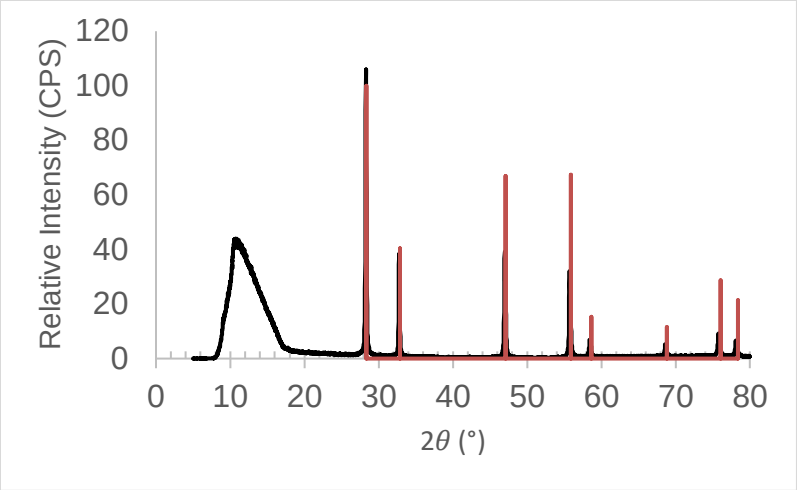

Figure S1. XRD pattern for UO_2. Red line indicates ICDD reference pattern for UO_2 (ICDD 00-041-1422). The broad peak from 8º to 17º 2θ is attributed to the anoxic dome over the sample as it was analyzed.

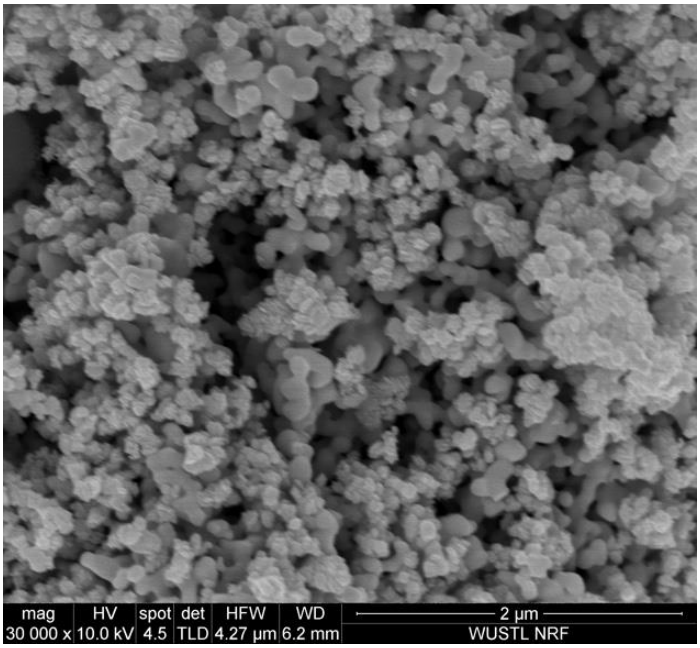

Figure S2. SEM image of UO_2.

HBED Inhibitory Effect at Low Ligand Concentration

At the low ligand concentration of 5 µM a clear inhibitory effect was seen for UO_2 solubilization (Figure S3). Consistently at all time points the U(IV) concentration in solution was suppressed by approximately 5 nM below that of the control (UO_2 with no ligand addition under same ionic strength and electrolyte composition).

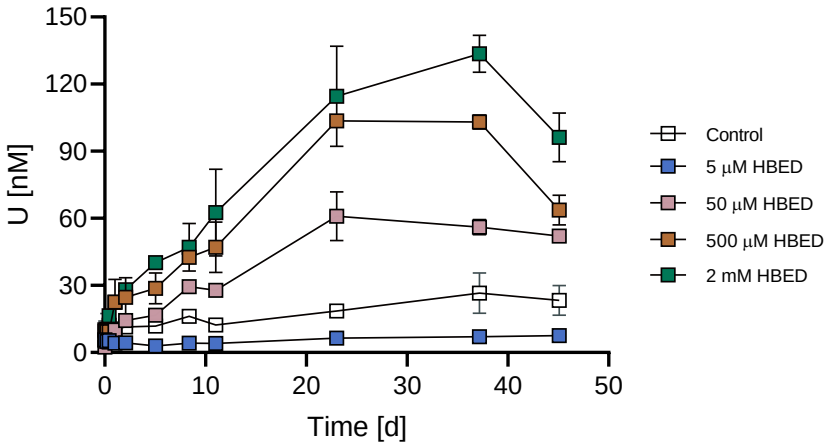

Figure S3. HBED-induced mobilization of UO_2 results. These results mimic those shown in Figure 1C but scaled to the extent of HBED mobilization to see in better resolution inhibitory effects seen at 5 μM ligand concentration.

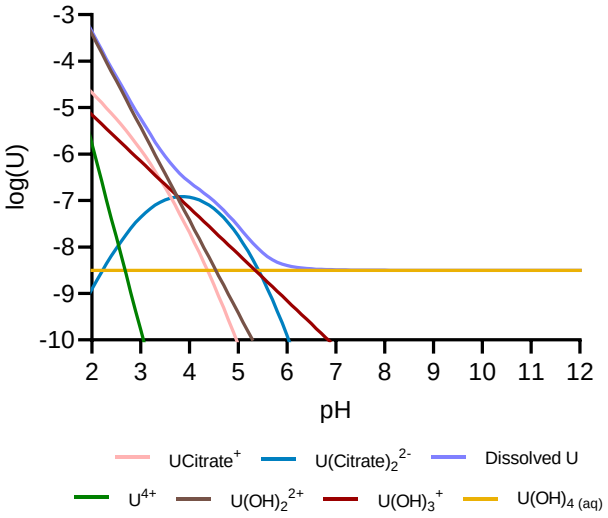

Figure S4. Equilibrium model of UO_2 solubility under experimental conditions (6.6 mM NaCl and 10 mM MOPS) with 2 mM citrate based off of the constants provided in **Error! Reference source not found.**. Model prepared in Visual MINTEQ.

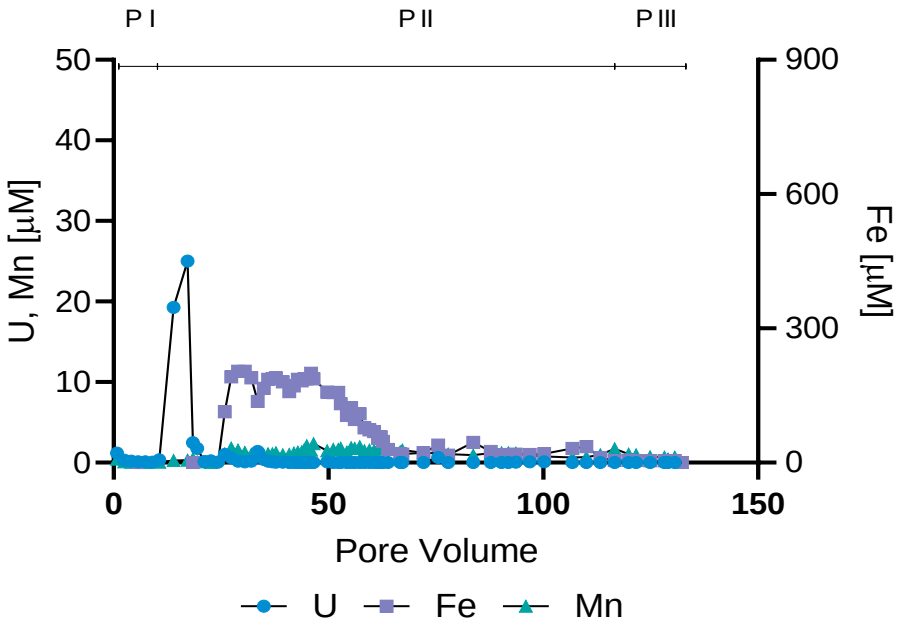

Figure S5. Uranium breakthrough and subsequent reduction in flow-through column experiment. P1 consisted of AGW solution. P2 consisted of AGW plus 4 mM glucose and 25 µM U. P3 consisted of AGW plus 4 mM glucose. At the end of P3 the column was promptly stored in an anaerobic chamber and sequestered along the column length before use in ligand batch experiments and sediment characterization work. All influent solutions were sparged with $CO_{2(g)}$ to pH 7.1 and pumped into anoxic gas-tight bags. Full influent solution compositions are summarized in Table 1.

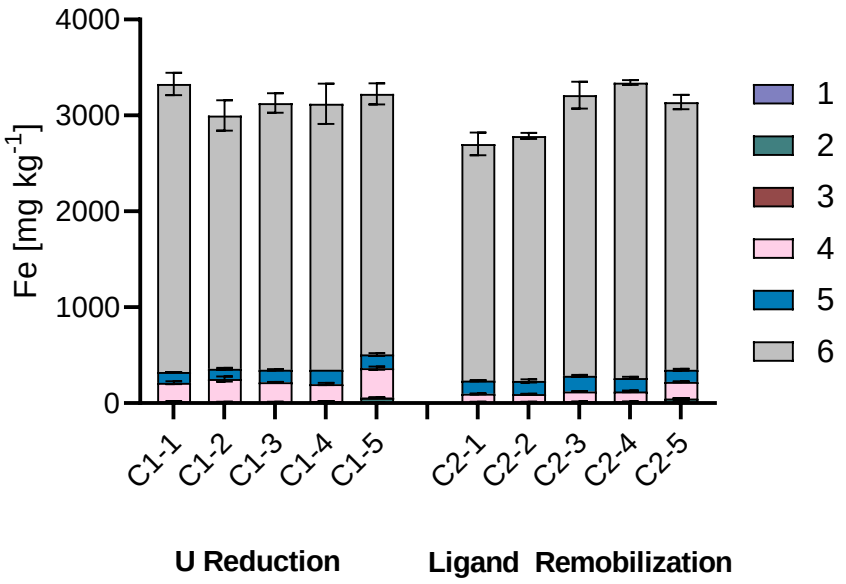

Figure S6. Iron sequential extraction for U reduction column and column after ligand remobilization. Error bars indicate standard deviation of triplicate reactors. Extractant solutions, SSR, and durations of each step are summarized in Table 2.

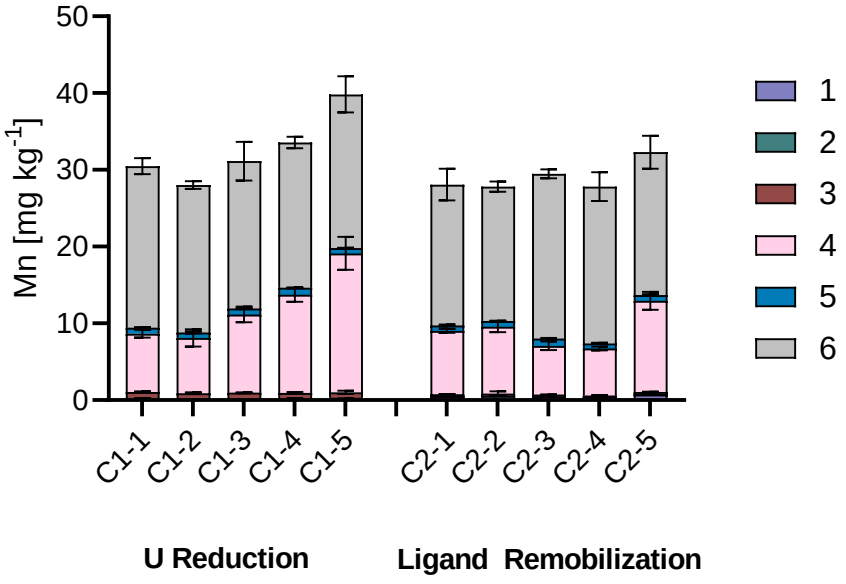

Figure S7. Manganese sequential extraction for U reduction column and column after ligand remobilization. Error bars indicate standard deviation of triplicate reactors. Extractant solutions, SSR, and durations of each step are summarized in Table 2.

Acknowledgements

To Anshuman Satpathy for his help in synthesizing UO_2, being my go-to person for research questions and brainstorming, as well as just being a great friend.

To Mario Alvarez for his invaluable work. I could not have asked for a better Master student to work alongside me.

To Stephan Kraemer, thank you for your guidance and always pushing me to learn more and deepen my understanding and critical thinking.

To Walter Schenkeveld and Naresh Kumar for their continued insights, support, and willingness to make time whenever I was stuck along the way.

To Dan Giammar, thank you for your hospitality in welcoming me into your lab group. For your mentorship and furthering of my scientific mind, I am greatly appreciative.

I would also like to thank Yvonne Roebbert for assistance in the non-crystalline U(IV) synthesis method, Jeffrey Czajka for assistance in bacterial inoculation and handling, as well as all the members of both the Giammar and Kraemer lab groups for their support and friendship.

And last but most certainly not least, thank you to Martina Kerndl for being my support system and life partner throughout this project.

References

1. Riley, R. G.; Zachara, J. *Chemical contaminants on DOE lands and selection of contaminant mixtures for subsurface science research*; Pacific Northwest Lab., Richland, WA (United States): 1992.

2. Abdelouas, A., Uranium mill tailings: geochemistry, mineralogy, and environmental impact. *Elements* **2006,** *2*, (6), 335-341.

3. Liesch, T.; Hinrichsen, S.; Goldscheider, N., Uranium in groundwater—fertilizers versus geogenic sources. *Science of the Total Environment* **2015,** *536*, 981-995.

4. WHO, Guidelines for drinking-water quality: fourth edition incorporating the first addendum. Geneva: World Health Organization; 2017. License: CC BY-NC-SA 3.0 IGO. **2017**.

5. Langmuir, D., *Aqueous environmental*. Prentice Hall: 1997.

6. Lovley, D. R.; Phillips, E. J.; Gorby, Y. A.; Landa, E. R., Microbial reduction of uranium. *Nature* **1991,** *350*, (6317), 413.

7. Löffler, F. E.; Edwards, E. A., Harnessing microbial activities for environmental cleanup. *Current Opinion in Biotechnology* **2006,** *17*, (3), 274-284.

8. Finneran, K. T.; Anderson, R. T.; Nevin, K. P.; Lovley, D. R., Potential for bioremediation of uranium-contaminated aquifers with microbial U (VI) reduction. *Soil and Sediment Contamination: An International Journal* **2002,** *11*, (3), 339-357.

9. Anderson, R. T.; Vrionis, H. A.; Ortiz-Bernad, I.; Resch, C. T.; Long, P. E.; Dayvault, R.; Karp, K.; Marutzky, S.; Metzler, D. R.; Peacock, A., Stimulating the in situ activity of Geobacter species to remove uranium from the groundwater of a uranium-contaminated aquifer. *Applied and environmental microbiology* **2003,** *69*, (10), 5884-5891.

10. Maher, K.; Bargar, J. R.; Brown Jr, G. E., Environmental speciation of actinides. *Inorganic chemistry* **2012,** *52*, (7), 3510-3532.

11. Williams, K. H.; Long, P. E.; Davis, J. A.; Wilkins, M. J.; N'Guessan, A. L.; Steefel, C. I.; Yang, L.; Newcomer, D.; Spane, F. A.; Kerkhof, L. J., Acetate availability and its influence on sustainable bioremediation of uranium-contaminated groundwater. *Geomicrobiology Journal* **2011,** *28*, (5-6), 519-539.

12. Yabusaki, S. B.; Fang, Y.; Long, P. E.; Resch, C. T.; Peacock, A. D.; Komlos, J.; Jaffe, P. R.; Morrison, S. J.; Dayvault, R. D.; White, D. C., Uranium removal from groundwater via in situ biostimulation: Field-scale modeling of transport and biological processes. *Journal of contaminant hydrology* **2007,** *93*, (1-4), 216-235.

13. Bargar, J. R.; Bernier-Latmani, R.; Giammar, D. E.; Tebo, B. M., Biogenic uraninite nanoparticles and their importance for uranium remediation. *Elements* **2008,** *4*, (6), 407-412.

14. Campbell, K. M.; Veeramani, H.; Ulrich, K.-U.; Blue, L. Y.; Giammar, D. E.; Bernier-Latmani, R.; Stubbs, J. E.; Suvorova, E.; Yabusaki, S.; Lezama-Pacheco, J. S., Oxidative dissolution of biogenic uraninite in groundwater at Old Rifle, CO. *Environmental science & technology* **2011,** *45*, (20), 8748-8754.

15. Shoesmith, D., Fuel corrosion processes under waste disposal conditions. *Journal of Nuclear Materials* **2000,** *282*, (1), 1-31.

16. Ludwig, K. R.; Grauch, R. I., Coexisting coffinite and uraninite in some sandstone-host uranium ores of Wyoming. *Economic Geology* **1980,** *75*, (2), 296-302.

17. De Pablo, J.; Casas, I.; Gimenez, J.; Marti, V.; Torrero, M., Solid surface evolution model to predict uranium release from unirradiated UO2 and nuclear spent fuel dissolution under oxidizing conditions. *Journal of nuclear materials* **1996,** *232*, (2-3), 138-145.

18. Ulrich, K.-U.; Ilton, E. S.; Veeramani, H.; Sharp, J. O.; Bernier-Latmani, R.; Schofield, E. J.; Bargar, J. R.; Giammar, D. E., Comparative dissolution kinetics of biogenic and chemogenic uraninite under oxidizing conditions in the presence of carbonate. *Geochimica et Cosmochimica Acta* **2009,** *73*, (20), 6065-6083.

19. Moon, H. S.; Komlos, J.; Jaffé, P. R., Uranium reoxidation in previously bioreduced sediment by dissolved oxygen and nitrate. *Environmental Science & Technology* **2007,** *41*, (13), 4587-4592.

20. Wang, Z.; Lee, S.-W.; Kapoor, P.; Tebo, B. M.; Giammar, D. E., Uraninite oxidation and dissolution induced by manganese oxide: A redox reaction between two insoluble minerals. *Geochimica et Cosmochimica Acta* **2013,** *100*, 24-40.

21. Bernier-Latmani, R.; Veeramani, H.; Vecchia, E. D.; Junier, P.; Lezama-Pacheco, J. S.; Suvorova, E. I.; Sharp, J. O.; Wigginton, N. S.; Bargar, J. R., Non-uraninite products of microbial U (VI) reduction. *Environmental science & technology* **2010,** *44*, (24), 9456-9462.

22. Wang, Y.; Frutschi, M.; Suvorova, E.; Phrommavanh, V.; Descostes, M.; Osman, A. A.; Geipel, G.; Bernier-Latmani, R., Mobile uranium (IV)-bearing colloids in a mining-impacted wetland. *Nature communications* **2013,** *4*, 2942.

23. Alessi, D. S.; Lezama-Pacheco, J. S.; Stubbs, J. E.; Janousch, M.; Bargar, J. R.; Persson, P.; Bernier-Latmani, R., The product of microbial uranium reduction includes multiple species with U (IV)–phosphate coordination. *Geochimica et Cosmochimica Acta* **2014,** *131*, 115-127.

24. Cerrato, J. M.; Ashner, M. N.; Alessi, D. S.; Lezama-Pacheco, J. S.; Bernier-Latmani, R.; Bargar, J. R.; Giammar, D. E., Relative reactivity of biogenic and chemogenic uraninite and biogenic noncrystalline U (IV). *Environmental science & technology* **2013,** *47*, (17), 9756-9763.

25. Loreggian, L.; Sorwat, J.; Byrne, J. M.; Kappler, A.; Bernier-Latmani, R., Role of Iron Sulfide Phases in the Stability of Noncrystalline Tetravalent Uranium in Sediments. *Environmental Science & Technology* **2020,** *54*, (8), 4840-4846.

26. Loreggian, L.; Novotny, A.; Bretagne, S. L.; Bartova, B.; Wang, Y.; Bernier-Latmani, R., Effect of Aging on the Stability of Microbially Reduced Uranium in Natural Sediment. *Environmental science & technology* **2019,** *54*, (1), 613-620.

27. Regenspurg, S.; Margot-Roquier, C.; Harfouche, M.; Froidevaux, P.; Steinmann, P.; Junier, P.; Bernier-Latmani, R., Speciation of naturally-accumulated uranium in an organic-rich soil of an alpine region (Switzerland). *Geochimica et Cosmochimica Acta* **2010,** *74*, (7), 2082-2098.

28. Bargar, J. R.; Williams, K. H.; Campbell, K. M.; Long, P. E.; Stubbs, J. E.; Suvorova, E. I.; Lezama-Pacheco, J. S.; Alessi, D. S.; Stylo, M.; Webb, S. M., Uranium redox transition pathways in acetate-amended sediments. *Proceedings of the National Academy of Sciences* **2013**, 201219198.

29. Sharp, J. O.; Lezama-Pacheco, J. S.; Schofield, E. J.; Junier, P.; Ulrich, K.-U.; Chinni, S.; Veeramani, H.; Margot-Roquier, C.; Webb, S. M.; Tebo, B. M., Uranium speciation and stability after reductive immobilization in aquifer sediments. *Geochimica et Cosmochimica Acta* **2011,** *75*, (21), 6497-6510.

30. Stoliker, D. L.; Campbell, K. M.; Fox, P. M.; Singer, D. M.; Kaviani, N.; Carey, M.; Peck, N. E.; Bargar, J. R.; Kent, D. B.; Davis, J. A., Evaluating chemical extraction techniques for the determination of uranium oxidation state in reduced aquifer sediments. *Environmental science & technology* **2013,** *47*, (16), 9225-9232.

31. Brainard, J. R.; Strietelmeier, B. A.; Smith, P. H.; Langston-Unkefer, P. J.; Barr, M. E.; Ryan, R. R., Actinide binding and solubilization by microbial siderophores. *Radiochimica Acta* **1992,** *58*, (2), 357-364.

32. Frazier, S. W.; Kretzschmar, R.; Kraemer, S. M., Bacterial siderophores promote dissolution of UO2 under reducing conditions. *Environmental science & technology* **2005,** *39*, (15), 5709-5715.

33. Luo, W.; Gu, B., Dissolution of uranium-bearing minerals and mobilization of uranium by organic ligands in a biologically reduced sediment. *Environmental science & technology* **2011,** *45*, (7), 2994-2999.

34. Boukhalfa, H.; Crumbliss, A. L., Chemical aspects of siderophore mediated iron transport. *Biometals* **2002,** *15*, (4), 325-339.

35. Church, B. D.; Halvorson, H., Dependence of the heat resistance of bacterial endospores on their dipicolinic acid content. *Nature* **1959,** *183*, (4654), 124-125.

36. Setlow, P., Spores of Bacillus subtilis: their resistance to and killing by radiation, heat and chemicals. *Journal of applied microbiology* **2006,** *101*, (3), 514-525.

37. Hoyt, H. L.; Gewanter, H. L., Citrate. In *Detergents*, Springer: 1992; pp 229-242.

38. López-Rayo, S.; Hernandez, D.; Lucena, J. J., Chemical evaluation of HBED/Fe3+ and the novel HJB/Fe3+ chelates as fertilizers to alleviate iron chlorosis. *Journal of agricultural and food chemistry* **2009,** *57*, (18), 8504-8513.

39. Ulrich, K.-U.; Singh, A.; Schofield, E. J.; Bargar, J. R.; Veeramani, H.; Sharp, J. O.; Bernier-Latmani, R.; Giammar, D. E., Dissolution of biogenic and synthetic UO2 under varied reducing conditions. *Environmental science & technology* **2008,** *42*, (15), 5600-5606.

40. Stylo, M.; Alessi, D. S.; Shao, P. P.; Lezama-Pacheco, J. S.; Bargar, J. R.; Bernier-Latmani, R., Biogeochemical controls on the product of microbial U (VI) reduction. *Environmental science & technology* **2013,** *47*, (21), 12351-12358.

41. Wasserstein, B., Ages of uraninites by a new method. *Nature* **1954,** *174*, (4439), 1004-1005.

42. Wang, Z.; Tebo, B. M.; Giammar, D. E., Effects of Mn (II) on UO2 dissolution under anoxic and oxic conditions. *Environmental science & technology* **2014,** *48*, (10), 5546-5554.

43. Wang, Y.; Frutschi, M.; Suvorova, E.; Phrommavanh, V.; Descostes, M.; Osman, A. A.; Geipel, G.; Bernier-Latmani, R., Mobile uranium (IV)-bearing colloids in a mining-impacted wetland. *Nature communications* **2013,** *4*, (1), 1-9.

44. Alessi, D. S.; Uster, B.; Veeramani, H.; Suvorova, E. I.; Lezama-Pacheco, J. S.; Stubbs, J. E.; Bargar, J. R.; Bernier-Latmani, R., Quantitative separation of monomeric U (IV) from UO2 in products of U (VI) reduction. *Environmental science & technology* **2012,** *46*, (11), 6150-6157.

45. Furrer, G.; Stumm, W., The coordination chemistry of weathering: I. Dissolution kinetics of δ-Al2O3 and BeO. *Geochimica et Cosmochimica Acta* **1986,** *50*, (9), 1847-1860.

46. Reichard, P.; Kraemer, S. M.; Frazier, S.; Kretzschmar, R., Goethite dissolution in the presence of phytosiderophores: rates, mechanisms, and the synergistic effect of oxalate. *Plant and Soil* **2005,** *276*, (1-2), 115-132.

47. Noël, V.; Boye, K.; Kukkadapu, R. K.; Li, Q.; Bargar, J. R., Uranium storage mechanisms in wet-dry redox cycled sediments. *Water research* **2019,** *152*, 251-263.

48. Jew, A. D.; Besançon, C. J.; Roycroft, S. J.; Noel, V. S.; Bargar, J. R.; Brown Jr, G. E., Chemical Speciation and Stability of Uranium in Unconventional Shales: Impact of Hydraulic Fracture Fluid. *Environmental science & technology* **2020,** *54*, (12), 7320-7329.

49. Schenkeveld, W.; Kimber, R. L.; Walter, M.; Oburger, E.; Puschenreiter, M.; Kraemer, S., Experimental considerations in metal mobilization from soil by chelating ligands: the influence of soil-solution ratio and pre-equilibration–a case study on Fe acquisition by phytosiderophores. *Science of the Total Environment* **2017,** *579*, 1831-1842.

50. Andreev, G. B.; Budantseva, N. A.; Fedoseev, A. M., Coordination interaction of transuranium elements with N-donor ligands. In *Structural Chemistry of Inorganic Actinide Compounds*, Elsevier: 2007; pp 363-407.

51. Chandrasekar, A.; Ghanty, T. K., Uncovering Heavy Actinide Covalency: Implications for Minor Actinide Partitioning. *Inorganic chemistry* **2019,** *58*, (6), 3744-3753.

52. Haddad, S.; Al-Far, R.; Ahmed, F., Structure of a neutral uranium (IV)–dipicolinic acid complex. *Acta Crystallographica Section C: Crystal Structure Communications* **1987,** *43*, (3), 453-456.

53. Loiseau, T.; Mihalcea, I.; Henry, N.; Volkringer, C., The crystal chemistry of uranium carboxylates. *Coordination Chemistry Reviews* **2014,** *266*, 69-109.

54. Bonin, L.; Cote, G.; Moisy, P., Speciation of An (IV)(Pu, Np, U and Th) in citrate media. *Radiochimica Acta* **2008,** *96*, (3), 145-152.

55. Hummel, W.; Mompean, F. J.; Illemassène, M.; Perrone, J., *Chemical thermodynamics of compounds and complexes of U, Np, Pu, Am, Tc, Se, Ni and Zr with selected organic ligands*. Elsevier Amsterdam: 2005; Vol. 9.

56. Luo, W.; Gu, B., Dissolution and mobilization of uranium in a reduced sediment by natural humic substances under anaerobic conditions. *Environmental science & technology* **2009,** *43*, (1), 152-156.

57. Pearson, R. G., Hard and soft acids and bases. *Journal of the American Chemical society* **1963,** *85*, (22), 3533-3539.

58. Kraemer, S. M.; Duckworth, O. W.; Harrington, J. M.; Schenkeveld, W. D., Metallophores and trace metal biogeochemistry. *Aquatic geochemistry* **2015,** *21*, (2-4), 159-195.

59. Maurice, P. A., *Environmental surfaces and interfaces from the nanoscale to the global scale*. Wiley: 2009.

60. Olsson, M.; Jakobsson, A.-M.; Albinsson, Y., Surface charge densities of two actinide (IV) oxides: UO2 and ThO2. *Journal of colloid and interface science* **2002,** *256*, (2), 256-261.

61. Borch, T.; Kretzschmar, R.; Kappler, A.; Cappellen, P. V.; Ginder-Vogel, M.; Voegelin, A.; Campbell, K., Biogeochemical redox processes and their impact on contaminant dynamics. *Environmental science & technology* **2010,** *44*, (1), 15-23.

62. Organization, W. H., *Guidelines for drinking-water quality*. World Health Organization: 1993.

63. Seitz, W.; Schulz, W.; Fischeder, R., Neue gesetzliche Vorgaben, Forschungsergebnisse und Konzepte zur Roh-und Trinkwasserüberwachung.

64. Guillaumont, R.; Mompean, F. J., *Update on the chemical thermodynamics of uranium, neptunium, plutonium, americium and technetium*. Elsevier Amsterdam: 2003; Vol. 5.